Cyano or o-nitrophenyl? Which is the optimal electron-withdrawing group for the acrylic acid acceptor of D-π-A sensitizers in DSSCs? A density functional evaluation

Ji Zhang · Yu-He Kan · Hai-Bin Li · Yun Geng · Yong Wu · Yu-Ai Duan · Zhong-Min Su

Abstract We report a DFT, TDDFT and DFTB investigation of the performance of two donor-π-acceptor (D-π-A)-type organic dyes bearing different electron-withdrawing groups (EWG) for dye-sensitized solar cells (DSSCs) to evaluate which EWG is better for an acrylic acid acceptor, i.e., Cyano (–CN) or o-nitrophenyl (o-NO$_2$–Ph). A series of theoretical criteria applied successfully in our previous work to explain the different performance of organic dyes related to open-circuit photovoltage (V_{oc}) and short-circuit current density (J_{sc}) were used to evaluate the performance of the dyes with just different EWG. Our calculated results reveal that dye **2** with o-NO$_2$–Ph has a larger vertical dipole moment, more electrons transferred from the dye to the semiconductor and a lower degree of charge recombination, which could lead to larger V_{oc}; while the larger driving force and comparable light harvesting efficiency could lead to higher J_{sc} , highlighting the potential of o-NO$_2$–Ph as an EWG in an acrylic acid acceptor.

Keywords Organic dye · Dye sensitized solar cell · Electron-withdrawing group · Electron transfer · Charge recombination · DFT

J. Zhang · Y.-H. Kan · H.-B. Li · Y. Geng · Y. Wu · Y.-A. Duan · Z.-M. Su (✉)
Institute of Functional Material Chemistry, Faculty of Chemistry, Northeast Normal University, Chang Chun 130024, Jilin, People's Republic of China
e-mail: zmsu@nenu.edu.cn

Y.-H. Kan
Jiangsu Key Laboratory for Chemistry of Low-Dimensional Materials, School of Chemistry and Chemical Engineering, Huaiyin Normal University, Huaian 223300, People's Republic of China

Introduction

As the global energy crisis and environment pollution become more and more serious, sources of clean and renewable solar energy have attracted tremendous attention from people all over the world. Dye-sensitized solar cells (DSSCs) have emerged at this historic moment due to their intriguing low-cost conversion of photovoltaic energy compared with conventional silicon-based semiconductor photovoltaic devices [1–3]. As dyes are the key component of a DSSC, dye optimization has become an effective way to improve the performance of these devices [4–6].

In general, mainly two types of dyes are used in DSSCs: ruthenium (Ru) polypyridyl dyes and metal-free organic dyes. Although the conversion efficiency of a cell based on metal-free organic dyes has reached 10.3 % [7], it is still lower than that of solar cells based on Ru complex photosensitizers, which have achieved conversion efficiencies of up to 11 % [8]. As a result, much effort has been done focusing on metal-free organic dyes with a view to improving their efficiency considering their high molar extinction coefficient, relatively low preparation costs and environmentally friendly rules. Most reported organic dyes adopt the donor–π spacer–acceptor (D-π-A) structural motif to improve the efficiency of intramolecular charge transfer (ICT) and thus enhance the efficiency of electron injection from the excited dye to the semiconductor. This structural motif is also very attractive due to the fact that its properties are easily tunable through modification of each component, i.e., donor, π spacer or acceptor part. In this respect, a mass of organic dyes featuring various donors such as triphenyl-amine (TPA) [9], carbazole [10], π spacer such as –C=C-chains [11], thiophene units (and derivatives) [12] and acceptor groups such as cyanoacrylic acid and rhodanine-3-acetic acid [13] has been synthesized and tested with the

purpose of improving the efficiency of the cell. With such a wide spectrum of organic dyes, there is an urgent need to clarify the structure–performance relationship to rapidly screen efficient dyes. There is no doubt that quantum chemical calculations manifest themselves as reliable and powerful tools to resolve this problem [14–16].

As we know, the acceptor group anchors the dye onto the semiconductor surface directly and plays a key role in dye anchoring, optical absorption, and electron-transfer processes. It is also well known that cyanoacrylic acid has been employed extensively as acceptor/anchor group successfully in most D-π-A dyes used at present, due to its strong electron-withdrawing capacity and the steady interaction with the semiconductor surface. This extensive use of the cyano (–CN) group in DSSCs naturally raises the question of whether –CN is the optimal electron-withdrawing group (EWG) for the acrylic acid acceptor. And, could any other EWG be used as an alternative? To the best of our knowledge, only scant effort has been devoted to replace –CN with other EWGs in an attempt to improve the performance of these dyes, especially when considering theoretical studies [17, 18]. Recently, Han et al. [19] synthesized a series of triphenylamine-bithiophene-based organic dyes with different EWGs, including trifluoromethyl –CF_3, o-nitrophenyl -o-NO_2–Ph and p-nitrophenyl -p-NO_2–Ph, aiming to improve cell efficiency. They found that the EWG could affect the performance of the dye, and the cell sensitized by the dye with -o-NO_2–Ph showed the best performance, but whether -o-NO_2–Ph also performs better than the most commonly used –CN was not investigated in their studies, which attracted our interest. In this work, we aimed to use a series of theoretical criteria, which had been applied successfully in our previous work [20, 21] to explain the different performance of organic dyes related to open-circuit photovoltage (V_{oc}) and short-circuit current density (J_{sc}) through density functional theory (DFT) and time-dependent DFT (TD-DFT) calculations, to evaluate the performance of the dyes with –CN and -o-NO_2–Ph as the EWG (shown in Fig. 1), respectively. We hope that increased understanding of the relationship between structure and performance will accelerate the design and

screening of dyes, yielding more efficient DSSCs for experimentalists.

Computational details and theoretical methodology

Geometry optimization of the ground state of the pure dyes was performed at B3LYP/6-31G(d) level in gas phase [22]. Frequency calculations were performed at the same level of theory to confirm that the optimized geometry corresponds to a stationary point. Linear response TD-DFT calculations were performed with the conductor-like polarizable continuum model (CPCM) [23, 24] for simulating the absorption spectrum of the pure dyes using different XC functionals, including pure functional PBE [25], BP86 [26, 27], global hybrid B3LYP, B3PW91 [22, 26] and BHandHLYP [28], range-separated functional CAM-B3LYP [29], LC-BLYP [30], M062X [31], ωB97X [32] and ωB97XD [33], and the hybrid meta-GGA TPSSh [34]. The results given by TD-CPCM-ωB97X/6-31G(d) were in good agreement with experimental values in terms of the functional test of the transition energies based on the optimized ground state structure (vide infra). And the test calculation of solvent effects shown in Table S1 in the supporting information confirmed that the solvent effects on the ground state structure have only trifling indirect influences on the transition energy. For the dye-$(TiO_2)_6$ system, ground state geometry optimization in the gas phase was performed under B3LYP level with 6-31G(d) for non-metal atoms and LanL2DZ basis set for Ti atoms, following natural population analysis (NPA) to evaluate the number of photoinjected electrons. As for dye-I_2 systems, basis set superposition error (BSSE) to the binding energies was calculated by using the counterpoise method after optimizing the systems at M06-2X level with LanL2DZ basis set for I atom and 6-31G(d) basis set for other atoms. All the calculations discussed above were performed with the Gaussian 09 program package [35]. As for the geometry optimization of the ground state of $(TiO_2)_{38}$ anatase cluster and dye-$(TiO_2)_{38}$ systems in the gas phase, self-consistent-charge density-functional tight-binding (SCC-DFTB) theory [36] in the ADF package

Fig. 1 Chemical structures and geometries of dyes **1** and **2**. Geometries were optimized under the level of B3LYP/6-31G(d) in gas phase
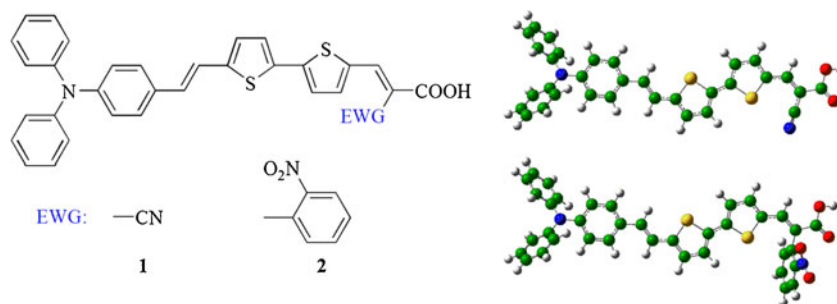
Table 1 Effects of the functional used on the lowest vertical excitation energy (Ex, eV) of **2** with the 6-31 G(d) basis set in acetonitrile solution. Data in parentheses are the corresponding results calculated in gas phase

Functional	PBE	B3LYP	B3PW91	BP86	LC-BLYP	EXP[a]
Ex	2.21 (2.36)	1.97 (2.22)	2.01 (2.23)	2.32 (2.41)	3.06 (3.15)	2.98
Functional	BHandHLYP	M062X	CAM-B3LYP	TPSSh	ωB97XD	ωB97X
Ex	2.65 (2.76)	2.69 (2.80)	2.70 (2.80)	2.62 (2.73)	2.78 (2.88)	2.94 (3.03)

[a] Experimental values from [19]

[37–39] was adopted, taking advantage of the efficiency of the DFTB method for optimizing large systems.

As we know, the energy conversion efficiency (η) of DSSCs can be determined as:

$$\eta = FF \frac{V_{oc} J_{sc}}{P_{inc.}} \quad (1)$$

where J_{sc} is the short-circuit current density, V_{oc} is the open-circuit photovoltage, FF is the fill factor, and $P_{inc.}$ is the intensity of the incident light.

J_{sc} is determined as:

$$J_{sc} = \int_{\lambda} LHE(\lambda) \Phi_{inject.} \eta_{collect.} d\lambda \quad (2)$$

where $\eta_{collect.}$ is the charge collection efficiency, for the same DSSCs differing only in the dye, as is the case for the organic dyes under study, it is reasonable to assume that $\eta_{collect.}$ is a constant. LHE(λ) is the light harvesting efficiency related to the oscillator strength (f) at a given wavelength. While the larger f, the stronger LHE [40]. Φ_{inject} is the electron injection efficiency, which is related to the driving force (ΔG_{inj}) of the electron injection from the photoinduced excited states of organic dyes to the semiconductor surface and the electronic coupling between the dye's LUMO and the semiconductor conduction band. In general, the larger ΔG_{inj} and electronic coupling, the larger the Φ_{inject}, and ΔG_{inj} (in eV) can usually be expressed as [41]:

$$\Delta G_{inj.} = E^{dye*} - E_c \quad (3)$$

where E_C is the reduction potential of the conduction band of the semiconductor, which is sensitive to the conditions, and the experimental value −4.00 eV (vs vacuum) is used widely [42]. E^{dye*} is the excited state oxidation potential of the organic dye, which is determined by the redox potential of the ground state of the dye (E^{dye}) and the vertical transition energy (λ_{max}), i.e., $E^{dye*} = E^{dye} - \lambda_{max}$ [41] when the electron injection from the photoinduced excited states of organic dyes to the semiconductor occurs before the vibrational relaxation [43–45]. For E^{dye}, this was evaluated at CPCM-(U) B3LYP/6-31G(d) for non-metal atoms and LanL2DZ for Ti atom level with the geometry of dye-(TiO$_2$)$_6$ cluster.

V_{oc} in DSSC can be determined by [46]:

$$V_{oc} = \frac{E_c}{q} + \frac{kT}{q} \ln\left(\frac{n_c}{N_{CB}}\right) - \frac{E_{redox}}{q} \quad (4)$$

In Eq. (4), kT and q are constants, representing the thermal energy and the unit charge, respectively. E_{redox} is the electrolyte Fermi-level and N_{CB} is the accessible density of conduction band states (7×10^{20} cm^{-3}) [47]. Here, we assume that they are constant too. n_c is the number of electrons in the conduction band. E_c is the conduction band edge of the semiconductor, and the shift of E_c [48] is in close connection with dipole moment of the dye as follows:

$$\Delta E_c = -\frac{q\mu_{normal}\gamma}{\varepsilon_0 \varepsilon} \quad (5)$$

Here, q is the electron charge; ε_0 and ε are the permittivity of the vacuum and the dielectric constant of the organic monolayer. γ is the dye's surface concentration, and μ_{normal}

Table 2 Computed maximum absorption wavelengths (λ_{max}), oscillator strengths (f), transition natures and the electron density difference maps of **1** and **2** corresponding to S$_0$→S$_1$ in acetonitrile by TD-ωB97X/6-31G(d) with B3LYP/6-31G(d) geometries

Dye	Main configurations[a]	λ_{max}[b] nm/eV	f	S$_0$→S$_1$[c]
1	HOMO-1→LUMO (0.32) HOMO→LUMO (0.52)	452/2.74 (431/2.88)	2.0174	
2	HOMO-1→LUMO (0.25) HOMO→LUMO (0.57)	422/2.94 (409/3.03)	2.0809	

[a] Data in parentheses are main configuration contributions

[b] Data in parentheses are the corresponding calculated results in gas phase

[c] Blue represents where the electrons are coming from, and white represents where the electrons are going

Table 3 Key parameters for deducing ΔG_{inj}

Dye	E^{dye} / eV	λ_{max} / eV	E^{dye*} /eV	$\Delta G_{inj.}$ / eV
1	4.88	2.49	2.39	−1.61
2	4.80	2.73	2.07	−1.93

is the component of dipole moment of the individual molecule perpendicular to the surface of semiconductor surface. It is obvious that a dye with a large μ_{normal} will induce a significant variation of V_{oc}.

Results and discussion

Previous works performed by us and Preat [6, 20, 21, 49–51] have confirmed that a suite of theoretical parameters, such as vertical dipole moment, electron numbers transferred from the dye to the semiconductor after photoexcitation and the extent of charge recombination affecting V_{oc}, light harvesting efficiency, injection driving force and the electronic coupling strength between the dye's LUMO and the semiconductor conduction band affecting J_{sc}, could be used successfully to rationalize and provide insight into the relationship between the structure and performance of organic dyes. Here, on the basis of these parameters, we attempt to shed light on the difference in efficiency of DSSCs based on these two dyes in order to develop more efficient EWGs.

Which EWG will have the larger J_{sc}?

Light harvesting efficiency

In a typical organic DSSC, the organic sensitizer fulfils the function of light absorption and injection of the photoexcited electrons to the conduction band of the semiconductor, thus the light harvesting efficiency (LHE) of the dyes is a critical

factor directly influencing J_{sc} as described in "Computational Details and Theoretical Methodology". In order to evaluate the LHE of the two dyes differing only in EWG, we first considered the functional effects on the vertical transition energy (Ex) of dye **2**, as we know that a judicious choice of functional is crucial to describe accurately the absorption spectrum of D-π-A dyes with non-negligible CT character [52, 53]. As shown in Table 1, the long-range-corrected (LC) functional, LC-BLYP and ωB97X with C-PCM solvent effects model yielded better results as compared with experimental data, with discrepancies of 0.08 and 0.04 eV, while other functionals underestimate the transition energy by more than 0.2 eV. We also tested the effects of other solvent models such as state-specified (SS) PCM on the transition energy of dye **2**, and the calculated results are listed in Table S2. We found that the SS-PCM model gives a little higher transition energy than the linear response C-PCM model, which is consistent with the finding of Jacquemin [54]. In addition, the SS-PCM gives more accurate results with discrepancies of 0.02 eV compared with the experimental results, with 0.04 eV for the C-PCM model. However, the SS-PCM calculations also need more computational time. Considering the compromise between computational costs and accuracy, we adopted the C-PCM solvent effects model. We used the ωB97X functional, 6-31G(d) basis set together with solvent effects of acetonitrile via the CPCM model to investigate the optical properties of the dyes in the following. The calculated maximum absorption wavelengths (λ_{max}), oscillator strengths (f), transition natures, electron density difference maps corresponding to $S_0 \rightarrow S_1$ are summarized in Table 2. We found that dyes **1** and **2** have comparable f, which could lead to similar LHE. The electron density difference maps of **1** and **2** corresponding to $S_0 \rightarrow S_1$ in acetonitrile solution plotted by GaussSum [55] demonstrated that, after photoexcitation, ICT occurs, i.e., the charge will transfer from triphenylamine through the vinyl bithiophene spacer to the acrylate acceptor, which would be beneficial for electron injection into the conduction band of TiO_2.

Fig. 2 Optimized geometrical structures of dyes **1** and **2** adsorbed onto the $(TiO_2)_{38}$ cluster

1@TiO₂ Side View   1@TiO₂ Front View   2@TiO₂ Side View   2@TiO₂ Front View
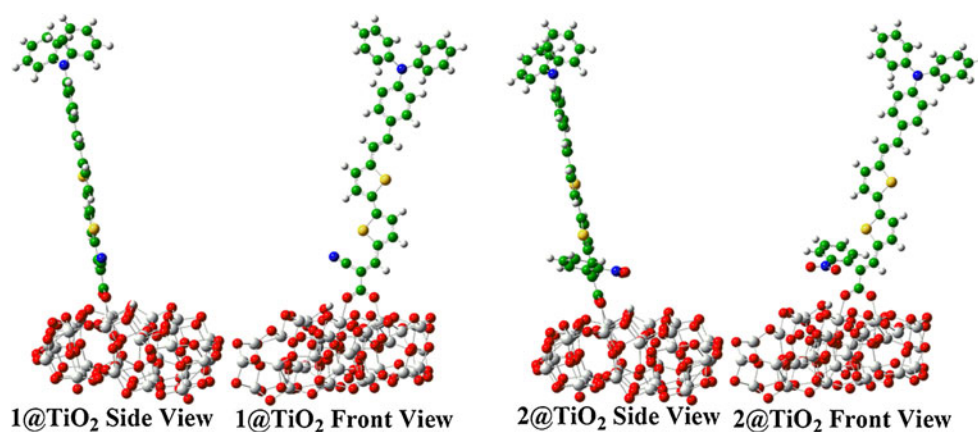
Driving force (ΔG_{inj}) and the electronic coupling strength

Considering the function of the dyes in the DSSC, besides the strong LHE, rapid and efficient electron injection after photo-excition is also very important for improving the efficiency of the cell. Thus, as discussed in "Computational Details and Theoretical Methodology", besides LHE, ΔG_{inj} and the electronic coupling strength affecting Φ_{inject} could also have effects on J_{sc}. Key parameters for deducing ΔG_{inj} are listed in Table 3. We found that both dyes have negative ΔG_{inj}, which means that the electron injection process is spontaneous, in good agreement with the energy level matching results discussed above. More importantly, we find that, compared with dye 1, dye 2 with -*o*-NO$_2$–Ph has the larger driving force. As in the discussion of the electronic coupling strength, we follow the conclusion from De Angelis et al. [56], who adopted the commonly used (TiO$_2$)$_{38}$ anatase cluster model to simulate the effect of the semiconductor and the bidentate bridging adsorption mode when the organic dye absorb onto the cluster. The initial geometry of the (TiO$_2$)$_{38}$ anatase cluster is shown in Fig. S1 in the supporting information. The geometries of dye-(TiO$_2$)$_{38}$ systems optimized by SCC-DFTB are shown in Fig. 2. In order to see which dye has the stronger electron coupling between the dye's LUMO and the semiconductor band, we analyzed the energy level of the dyes before and after interacting with the (TiO$_2$)$_{38}$ anatase cluster, as depicted in Fig. 3. From Fig. 3, we can draw some conclusions, including (1) the HOMO–LUMO gap of the considered

Fig. 4 Calculated vertical dipole moment of dyes **1** and **2** at CPCM-B3LYP/6-31G(d) level in acetonitrile solution. The semiconductor surface is parallel to the *yz* plane

(TiO$_2$)$_{38}$ anatase cluster computed by B3LYP/6-31G(d) for non-metal atoms and LanL2DZ for Ti atom//SCC-DFTB method is 3.72 eV, in good agreement with the experimental typical band gaps of TiO$_2$ nanoparticles of a few nanometers in size (3.2–3.3 eV) [57], confirming the reliability of the theoretical semiconductor model and method we used here; (2) the interaction between the dye and the semiconductor has almost no effects on the HOMO of the dye. The HOMO of the interaction system corresponds to the HOMO of the free dyes; (3) after interaction with TiO$_2$ surface, the position and character of the dye's LUMO are affected. For both dyes, the dye's

Fig. 3 Schematic energy diagram of the pure dyes, dye-(TiO$_2$)$_{38}$ systems and the (TiO$_2$)$_{38}$ model at the B3LYP level with 6-31G(d) for non-metal atoms and LanL2DZ basis set for Ti atom. The selective molecular orbitals are also shown with an isodensity surface of 0.02
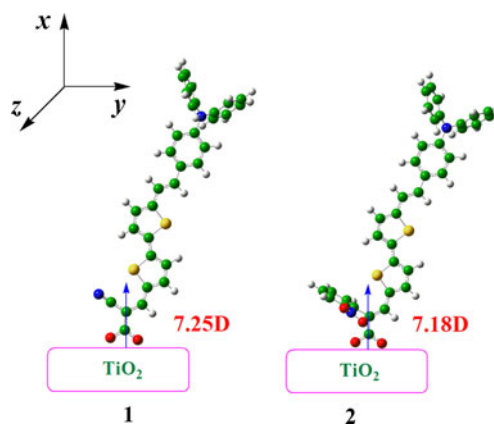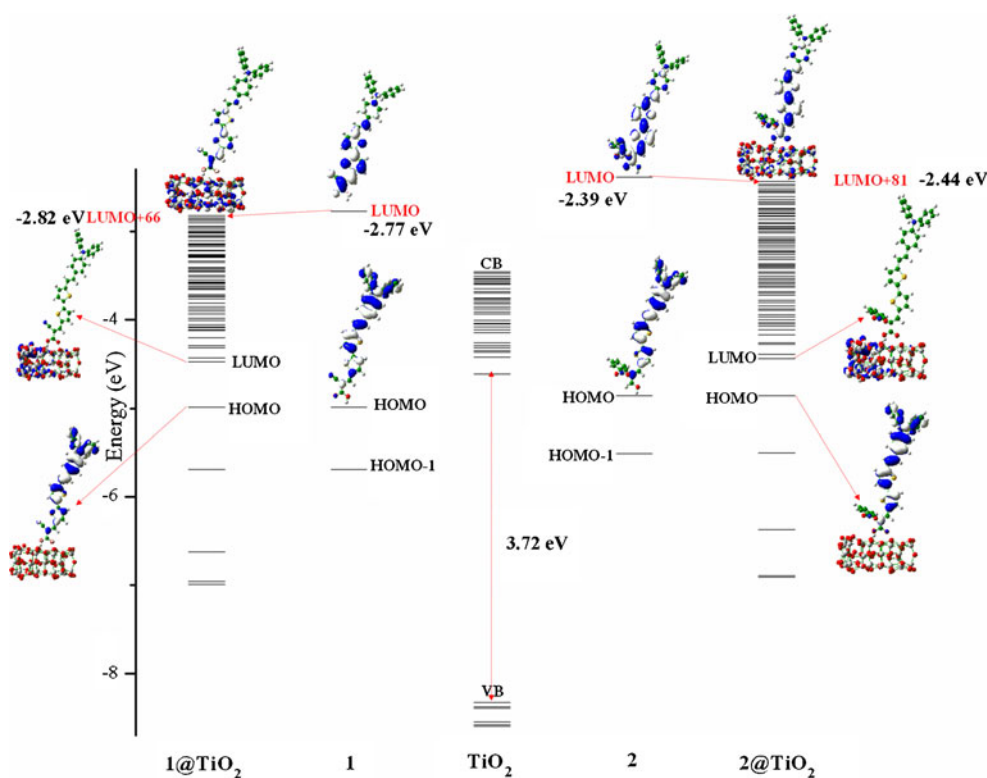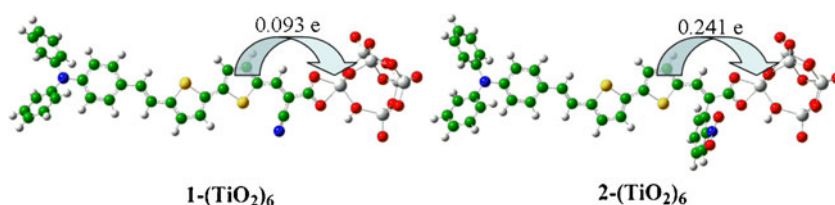
1-$(TiO_2)_6$ 2-$(TiO_2)_6$

LUMO is 0.05 eV lower after interaction with the TiO_2 surface, indicating similar electronic coupling strength between the organic dye and the semiconductor surface. Thus, we can draw the conclusion that, compared with dye **1**, dye **2** has larger LHE and ΔG_{inj}, but similar electronic coupling strength leading to larger J_{sc}.

Which EWG will have the larger V_{oc}?

Vertical dipole moment (μ_{normal})

We calculated the μ_{normal} of the dyes at B3LYP/6-31G(d) level including solvent effects by means of the CPCM model using the geometry of dyes adsorbed onto the $(TiO_2)_{38}$ cluster. We know (see "Computational Details and Theoretical Methodology") that the shift of the conduction band, which is related to μ_{normal} of the dyes, will lead to a change in V_{oc} [48]. It is generally accepted that the larger the μ_{normal} of the adsorbed molecules pointing outward from the semiconductor surface, the larger the V_{oc} [56, 58, 59]. Considering the bidentate binding mode of the dyes, we made the C_2 axis of the carboxylate in the dye parallel to the x-axis, and the semiconductor surface parallel to the yz plane. Thus, the orientations of the dyes after binding to the semiconductor are simulated. The dipole moment along the x-axis of the dyes is referred to as μ_{normal}. The calculated results at CPCM-B3LYP/6-31G(d) level with the geometry of dyes adsorbed onto the $(TiO_2)_{38}$ cluster are shown in Fig. 4; we found that these two dyes have similar μ_{normal} (7.25D for dye **1** and 7.18D for dye **2**), although the EWG was changed.

Electron number in the conduction band (n_c)

As discussed in "Computational Details and Theoretical Methodology", besides μ_{normal}, n_c is an important parameter affecting V_{oc}, which is a balance between the number of photoinjected electrons ($n_{c,inj}$) from the excited dye to the semiconductor and the number of electrons lost during the charge recombination ($n_{c,rec.}$). In order to calculate $n_{c,inj}$, we follow the conclusion of Sánchez-de-Armas et al. [60] using the $(TiO_2)_6$ nanocluster to simulate the semiconductor surface effects in view of the compromise between computational effort and accuracy. This nanocluster has proved suitable to simulate the features in the absorption spectra of the system. As for the adsorption configurations, Sánchez-de-Armas et al. [61] also demonstrated that the bidentate chelating adsorption mode is more energetically favorable than the bidentate bridging mode through theoretical calculations for the similar systems. As a result, we adopted the $(TiO_2)_6$ nanocluster taken from reference [62] and the bidentate chelating adsorption mode to investigate the dye-semiconductor interaction effects on absorption spectra properties. The optimized structures of the dye-$(TiO_2)_6$ clusters are shown in Fig. 5. Although the TiO_2 model used here may be somewhat too simple to simulate fully the effect of the semiconductor, our previous work [20] demonstrated the reliability of this model. Here, we performed NPA at the CPCM/B3LYP/6-31G(d) level for nonmetal atoms and LANL2DZ basis set for Ti atom level using NBO 3.1 in Gaussian 09 in the ground state (S_0) and first
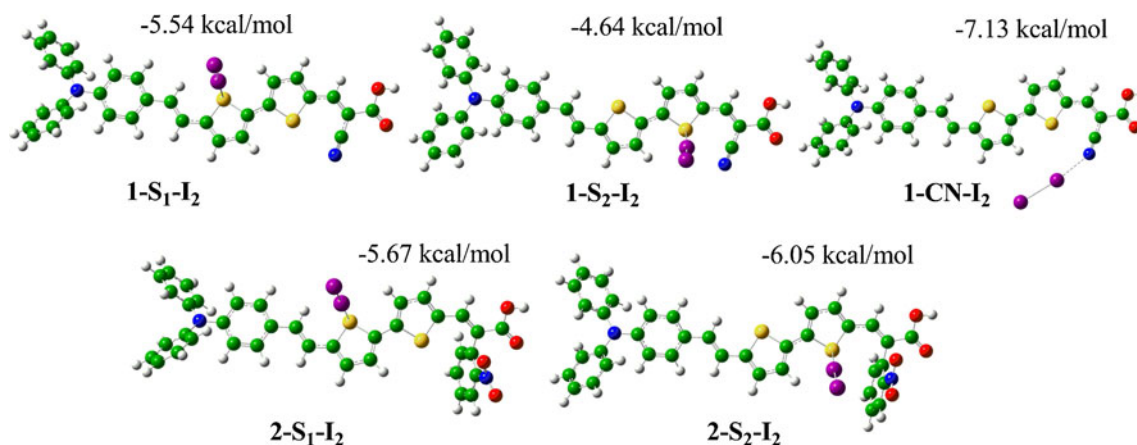

−5.54 kcal/mol   −4.64 kcal/mol   −7.13 kcal/mol

1-S_1-I_2 1-S_2-I_2 1-CN-I_2

−5.67 kcal/mol   −6.05 kcal/mol

2-S_1-I_2 2-S_2-I_2

Fig. 6 Optimized molecular structures of the dye–I_2 complexes under M062X/6-31G(d) (LanL2DZ basis set for I atom) level

singlet excited states (S_1) of the dye-$(TiO_2)_6$ cluster to qualitatively or semi-quantitatively determine $n_{c,inj}$. The calculated $n_{c,inj}$ shown in Fig. 5 is in the order of **2** (0.240 e) >**1** (0.092 e). We also used the Merz-Kollman method—demonstrated by Jacquemin et al. [63] to be the optimal atomic charge model for studying space charge-transfer excitations—to calculate the atomic charge distributions. The corresponding calculated results are listed in the Electronic Supplementary Information (Table S3). We find that, although the absolute values of $n_{c,inj}$ obtained from these two formalisms are different, the trend of $n_{c,inj}$ is consistent. So we think the results obtained here are reasonable.

As for other factors affecting n_c, i.e., charge recombination, because several groups have demonstrated that the possible halogen bonding between the special atoms of the dye and I_2 in the electrolyte could accelerate interfacial charge recombination through facilitating I_2 close to the semiconductor surface and improving the I_2 concentration in the vicinity of the TiO_2, we discussed the dye–I_2 interaction to see the EWG effects on the extent of charge recombination. The optimized geometries of the dye–I_2 complex under M06-2X/6-31G(d) (LanL2DZ basis set for I atom) level in gas phase are listed in Fig. 6. The binding energies, after BSSE correction, of I_2 with different electron donor sites on these molecules were calculated and listed in Fig. 6. Compared with dye **2**, dye **1** has one more interaction site to bond I_2, i.e., CN–I_2 interaction. On the other hand, we could also find that –CN has the strongest ability to bond I_2 due to the largest bonding energies (-7.13 kcal mol^{-1}), which could facilitate the approach of I_2 to the semiconductor surface, and thus accelerate interfacial charge recombination. When the –CN group is replaced by -o-NO_2-Ph in dye **2**, besides the fewer interaction sites to bond I_2, the steric orientation of o-NO_2–Ph could also efficiently block the approach of I_2 to the semiconductor surface and thus slow the interfacial charge recombination. It also gives us a hint that, besides reducing the interaction sites, we could also enhance the blocking effect of the dyes in the molecular design to improve cell efficiency. Thus, combining the μ_{normal}, $n_{c,inj}$ and the extent of the charge recombination, we could predict that dye **2** with o-NO_2–Ph should have larger V_{oc}, for it has larger $n_{c,inj}$, slower charge recombination and similar μ_{normal}.

Conclusions

The geometries, electronic structures and absorption spectra of two triphenylamine-bithiophene-based organic dyes with different electron-withdrawing groups (EWG) were evaluated through DFT, TDDFT and DFTB methods with the aim of gaining insights into the effects of the EWG on the performance of the dyes. Our calculated results pointed out that dye **2** with the o-nitrophenyl group has larger V_{oc} due to larger dipole moment, more electrons transferred from the dye to the semiconductor and lower charge recombination degree, while the larger driving force and comparable light harvesting efficiency lead to higher J_{sc}. Our results indicate that cyano may not be the optimal electron-withdrawing group for the acrylic acid acceptor of D-π-A sensitizers in DSSCs, and o-nitrophenyl could be used as a promising EWG candidate to improve the efficiency of these dyes. We hope that our investigation could pave the way to the design and screening of new efficient organic dyes with novel acceptors.

References

1. O'Regan B, Grätzel M (1991) Nature 353:737–740
2. Grätzel M (2001) Nature 414:338–344
3. Grätzel M (2003) J Photochem Photobiol C Photochem Rev 4:145–153
4. Horiuchi T, Miura H, Sumioka K, Uchida S (2004) J Am Chem Soc 126:12218–12219
5. Mishra A, Fischer MKR, Bäuerle P (2009) Angew Chem Int Ed 48:2474–2499
6. Preat J, Jacquemin D, Perpete EA (2010) Energy Environ Sci 3:891–904
7. Zeng W, Cao Y, Bai Y, Wang Y, Shi Y, Zhang M, Wang F, Pan C, Wang P (2010) Chem Mater 22:1915–1925
8. Cao Y, Bai Y, Yu Q, Cheng Y, Liu S, Shi D, Gao F, Wang P (2009) J Phys Chem C 113:6290–6297
9. Irfan A, Al-Sehemi AG, Asiri AM (2012) J Mol Model 18:3609–3615
10. Yakhanthip T, Jungsuttiwong S, Namuangruk S, Kungwan N, Promarak V, Sudyoadsuk T, Kochpradist P (2011) J Comput Chem 32:1568–1576
11. Liu J, Zhou D, Xu M, Jing X, Wang P (2011) Energy Environ Sci 4:3545–3551
12. Zhang G, Bai Y, Li R, Shi D, Wenger S, Zakeeruddin SM, Gratzel M, Wang P (2009) Energy Environ Sci 2:92–95
13. Marinado T, Hagberg DP, Hedlund M, Edvinsson T, Johansson EMJ, Boschloo G, Rensmo H, Brinck T, Sun L, Hagfeldt A (2009) Phys Chem Chem Phys 11:133–141
14. Cui H, Ma R, Guo P, Zeng Q, Liu G, Zhang X (2010) J Mol Model 16:303–310
15. Xu J, Zhu L, Wang L, Liu L, Bai Z, Xu W (2012) J Mol Model 18:1767–1777
16. Martsinovich N, Troisi A (2011) Energy Environ Sci 4:4473–4495
17. Srinivas K, Yesudas K, Bhanuprakash K, Rao VJ, Giribabu L (2009) J Phys Chem C 113:20117–20126
18. Meng S, Kaxiras E, Nazeeruddin MK, Grätzel M (2011) J Phys Chem C 115:9276–9282
19. Numata Y, Ashraful I, Shirai Y, Han L (2011) Chem Commun 47:6159–6161

20. Zhang J, Li H-B, Sun S-L, Geng Y, Wu Y, Su Z-M (2012) J Mater Chem 22:568–576
21. Zhang J, Kan Y-H, Li H-B, Geng Y, Wu Y, Su Z-M (2012) Dyes Pigments 95:313–321
22. Becke AD (1993) J Chem Phys 98:5648–5652
23. Cossi M, Rega N, Scalmani G, Barone V (2003) J Comput Chem 24:669–681
24. Cossi M (2001) J Chem Phys 115:4708
25. Perdew JP, Burke K, Ernzerhof M (1996) Phys Rev Lett 77:3865–3868
26. Becke AD (1988) Phys Rev A 38:3098
27. Lee C, Yang W, Parr RG (1988) Phys Rev B 37:785
28. Becke A (1993) J Chem Phys 98:1372
29. Yanai T, Tew DP, Handy NC (2004) Chem Phys Lett 393:51–57
30. Wong BM, Piacenza M, Sala FD (2009) Phys Chem Chem Phys 11:4498–4508
31. Zhao Y, Truhlar D (2008) Theor Chem Accounts 120:215–241
32. Chai JD, Head-Gordon M (2008) J Chem Phys 128:084106
33. Chai JD, Head-Gordon M (2008) Phys Chem Chem Phys 10:6615–6620
34. Staroverov VN, Scuseria GE, Tao J, Perdew JP (2003) J Chem Phys 119:12129–12137
35. Frisch MJ, Trucks GW, Schlegel HB, Scuseria GE, Robb MA, Cheeseman JR, Scalmani G, Barone V, Mennucci B, Petersson GA, Nakatsuji H, Caricato M, Li X, Hratchian HP, Izmaylov AF, Bloino J, Zheng G, Sonnenberg JL, Hada M, Ehara M, Toyota K, Fukuda R, Hasegawa J, Ishida M, Nakajima T, Honda Y, Kitao O, Nakai H, Vreven T, Montgomery JA Jr, Peralta JE, Ogliaro F, Bearpark M, Heyd JJ, Brothers E, Kudin KN, Staroverov VN, Kobayashi R, Normand J, Raghavachari K, Rendell A, Burant JC, Iyengar SS, Tomasi J, Cossi M, Rega N, Millam JM, Klene M, Knox JE, Cross JB, Bakken V, Adamo C, Jaramillo J, Gomperts R, Stratmann RE, Yazyev O, Austin AJ, Cammi R, Pomelli C, Ochterski JW, Martin RL, Morokuma K, Zakrzewski VG, Voth GA, Salvador P, Dannenberg JJ, Dapprich S, Daniels AD, Farkas O, Foresman JB, Ortiz JV, Cioslowski J, Fox DJ (2009) Gaussian 09W, Revision A.02. Gaussian, Inc, Wallingford CT
36. Elstner M, Porezag D, Jungnickel G, Elsner J, Haugk M, Frauenheim T, Suhai S, Seifert G (1998) Phys Rev B 58:7260–7268
37. Velde GT, Bickelhaupt FM, Baerends EJ, Fonseca Guerra C, van Gisbergen SJA, Snijders JG, Ziegler T (2001) J Comput Chem 22:931–967
38. Fonseca Guerra C, Snijders JG, Te Velde G, Baerends EJ (1998) Theor Chem Acc 99:391–403
39. 111 ADF20012.01, SCM. Theoretical Chemistry Vrije Universiteit Amsterdam.The Netherlands; http://www.scm.com
40. Nalwa HS (2001) Handbook of advanced electronic and photonic materials and devices. Academic, San Diego, CA
41. Katoh R, Furube A, Yoshihara T, Hara K, Fujihashi G, Takano S, Murata S, Arakawa H, Tachiya M (2004) J Phys Chem B 108:4818–4822
42. Asbury JB, Wang YQ, Hao E, Ghosh HN, Lian T (2001) Res Chem Intermed 27:393–406
43. Anderson NA, Ai X, Lian T (2003) J Phys Chem B 107:14414–14421
44. Ramakrishna G, Singh AK, Palit DK, Ghosh HN (2004) J Phys Chem B 108:4775–4783
45. Zimmermann C, Willig F, Ramakrishna S, Burfeindt B, Pettinger B, Eichberger R, Storck W (2001) J Phys Chem B 105:9245–9253
46. Marinado T, Nonomura K, Nissfolk J, Karlsson MK, Hagberg DP, Sun L, Mori S, Hagfeldt A (2010) Langmuir 26:2592–2598
47. Bai Y, Yu Q, Cai N, Wang Y, Zhang M, Wang P (2011) Chem Commun 47:4376–4378
48. Rühle S, Greenshtein M, Chen SG, Merson A, Pizem H, Sukenik CS, Cahen D, Zaban A (2005) J Phys Chem B 109:18907–18913
49. Preat J, Jacquemin D, Michaux C, Perpète EA (2010) Chem Phys 376:56–68
50. Preat J, Michaux C, Jacquemin D, Perpète EA (2009) J Phys Chem C 113:16821–16833
51. Ning Z, Fu Y, Tian H (2010) Energy Environ Sci 3:1170–1181
52. Adamo C, Jacquemin D (2013) Chem Soc Rev. doi:10.1039/c2cs35394f
53. Jin J-L, Li H-B, Geng Y, Wu Y, Duan Y-A, Su Z-M (2012) Chemphyschem 13:3714–3722
54. Chibani S, Le Guennic B, Charaf-Eddin A, Maury O, Andraud C, Jacquemin D (2012) J Chem Theory Comput 8:3303–3313
55. O'Boyle NM, Tenderholt AL, Langner KM (2008) J Comput Chem 29:839–845
56. Chen P, Yum JH, Angelis FD, Mosconi E, Fantacci S, Moon S-J, Baker RH, Ko J, Nazeeruddin MK, Grätzel M (2009) Nano Lett 9:2487–2492
57. Khoudiakov M, Parise AR, Brunschwig BS (2003) J Am Chem Soc 125:4637–4642
58. Peng B, Yang S, Li L, Cheng F, Chen J (2010) J Chem Phys 132:034305–034309
59. Liu B, Wu W, Li X, Li L, Guo S, Wei X, Zhu W, Liu Q (2011) Phys Chem Chem Phys 13:8985–8992
60. Sánchez-de-Armas RO, Oviedo López J, San-Miguel MA, Sanz JF, Ordejón P, Pruneda M (2010) J Chem Theory Comput 6:2856–2865
61. Sanchez-de-Armas R, San Miguel MA, Oviedo J, Sanz JF (2012) Phys Chem Chem Phys 14:225–233
62. Sanchez-de-Armas R, San-Miguel MA, Oviedo J, Marquez A, Sanz JF (2011) Phys Chem Chem Phys 13:1506–1514
63. Jacquemin D, Bahers TL, Adamo C, Ciofini I (2012) Phys Chem Chem Phys 14:5383–5388